IDENTIFICATION OF A SUPPRESSOR MUTANT OF SLC16A6A DEFICIENCY IN ZEBRAFISH, AND DEVELOPMENT OF TOOLS FOR STUDYING THE ROLE OF SLC16A6 IN MELANOMA

by

Erin Lu Dickson

A thesis submitted to the faculty of
The University of Utah
in partial fulfillment of the requirements for the degree of

Master of Science

Department of Biochemistry

The University of Utah

August 2015

The University of Utah Graduate School

STATEMENT OF THESIS APPROVAL

The thesis of **Erin Lu Dickson**

has been approved by the following supervisory committee members:

Amnon Schlegel	, Chair	**04/29/2015**
		Date Approved
Janet Lindsley	, Member	**04/29/2015**
		Date Approved
Jared Rutter	, Member	**04/29/2015**
		Date Approved

and by **Christopher P. Hill** , Chair/Dean of

the Department/College/School of **Biochemistry**

and by David B. Kieda, Dean of The Graduate School.

ABSTRACT

Obesity is a major burden on public health, responsible for a myriad of complicated, dysfunctional metabolic phenotypes. In particular, the accumulation of fat outside of adipocytes is a serious area of concern. Non-alcoholic fatty liver disease (NAFLD) is one such obesity-related disorder, about which little is known on a molecular level and for which successful treatment has yet to be established. My thesis lab took a genetic approach in zebrafish to identify new genes that participate in lipid metabolism in hope of finding mutants with ectopic lipid accumulation. A mutant with hepatic steatosis, or fatty liver, was identified. In this mutant, *red moon* (*rmn*), *slc16a6a* is nonfunctional, rendering hepatocytes unable to release ketone bodies during fasting. The trapped carbon atoms from these partially oxidized, short chain fatty acids critical to meeting the energy demands of the brain during starvation are diverted to *de novo* lipogenesis, and storage as triacylglycerol in cytoplasmic lipid droplets.

My thesis work begins to build on known aspects of *slc16a6a* function. I started with a genetic screen to identify dominant modifying mutants and have discovered one such mutation, *total eclipse of red moon* (*term)*, which suppresses the *slc16a6a*$^{-/-}$ phenotype. I have begun to determine its genomic position with RNA-seq mapping and have cloned several candidate genes. I have tested the candidates for mutations that could explain physiological insight into how hepatic steatosis can be attenuated. The hope is this new information can be used to develop novel therapeutic approaches to NAFLD.

I have also established a platform to evaluate this gene's role in a different disease context: cancer. Human melanomas show increased expression of *SLC16A6*. With Tol2 transgenesis techniques, I made a transgenic construct that will be used to test whether this gene promotes cancer, measuring tumor growth and metastasis. This begins to look at whether ketone body uptake is a significant aspect of melanoma metabolism. The outcome of experiments done on the platform I have established could reveal a novel therapeutic avenue for melanoma.

TABLE OF CONTENTS

ABSTRACT iii

LIST OF FIGURES vi

ABBREVIATIONS vii

ACKNOWLEDGEMENTS viii

CHAPTERS

1. INTRODUCTION 1

Non-alcoholic fatty liver disease 1
Solute carrier family 16a, member 6a 2
Approach for identification of new hepatic lipid metabolism genes 4
Monocarboxylate transporters in cancer 5

2. *total eclipse of red moon* 8

Genetic screening for dominant modifiers of *slc16a6a*$^{-/-}$ 8
Mutation mapping analysis using RNA-Seq) 9
Candidates for the *term* gene 10
Materials and methods 14

3. TRANSGENIC EXPRESSION OF HUMAN SLC16A6 18

Human SLC16A6 in mammalian cells 18
Transgenic SLC16A6 zebrafish 18
Future directions 21
Materials and methods 24

APPENDIX: PCR PRIMERS AND PARAMETERS 27

REFERENCES 29

LIST OF FIGURES

Figures

1 Whole mount staining of fixed 6 dpf larve stained with Oil Red O (ORO) 3

2 Affymetrix microarray of human skin samples 5

3 *total eclipse of red moon* 9

4 Single nucleotide polymorphisms segregating with *term* are clustered on chromosome 7.....11

5 Transgenic expression of SLC16A6 in mammalian cells.....19

6 Transgenic expression of SLC16A6 in zebrafish liver.....20

7 Transgenesis strategy to test *SLC16A6* involvement in melanoma 22

ABBREVIATIONS

NAFLD ..... non-alcoholic fatty liver disease
NASH ..... non-alcoholic steatohepatitis
rmn ..... *red moon*
dpf ..... days post fertilization
ORO ..... oil red O
slc16a6a ..... solute carrier protein family 16a, member 6a
MCT ..... monocarboxylate transporter
MMAPPR ..... mutation mapping analysis pipeline for pooled RNA-Seq
RNA-Seq ..... RNA sequencing
SNP ..... single nucleotide polymorphism
term ..... *total eclipse of red moon*
ENU ..... *N*-ethyl-*N*-nitrosourea
Mb ..... megabases
VLDL ..... very low-density lipoprotein
GWAS ..... genome-wide association study
PBS ..... phosphate buffered saline
PCR ..... polymerase chain reaction
RT-PCR ..... reverse transcriptase-polymerase chain reaction
LB ..... lysogeny broth
X-Gal 5-bromo-4-chloro-3-indolyl-β-D-galactopyranoside
IPTG ..... isopropyl β-D-1-thiogalactopyranoside
CHO ..... chinese hamster ovary
EGFP ..... enhanced green fluorescent protein
MAPKK ..... mitogen-activated protein kinase kinase
mRNA ..... messenger RNA

ACKNOWLEDGEMENTS

I would first like to acknowledge my thesis advisor, Amnon Schlegel, who has always put my education and my success high on his priority list. I thank him for his creative and important research questions and his willingness to entrust part of that work to me. I also thank my thesis committee, Janet Lindsley, Jared Rutter, Brenda Bass, and Kristen Kwan for their helpful questions, suggestions, and technical expertise they offered me in my research.

Next, I acknowledge my labmates who offered collaboration to me during my graduate career in the form of technical help and ideas: Sarah Hugo, Santhosh Karanth, Lourdes Cruz García, Tibiábin Benítez Santana, Madhukar Aryal, Holly Astin, and Nikita Abraham. I also thank countless other students and faculty who also participated in enriching my knowledge and experience, particularly members of the Molecular Biology/Biological Chemistry programs who entered in 2011 and 2012.

I also want to pay recognition to my faith community here in Salt Lake City for acting as witnesses of Jesus Christ, his love, his mercy, and his will. In particular, I thank Fr. Carl Schlichte, Fr. Peter Hannah, Jon Dalton, Vicki Turner, Jim Dotterweich, Katie Smith, and Nathaniel Binversie. I also acknowledge my family, Andrew, Kerstin, and John Dickson for their constant love and support throughout my life. Finally, I acknowledge the triune God, my creator and redeemer, without whom nothing is possible. I thank him, his blessed mother, and his saints for my life and all other gifts.

CHAPTER 1

INTRODUCTION

Non-alcoholic fatty liver disease

Obesity is an alarmingly prevalent and continually worsening problem worldwide. It also provokes and aggravates other metabolic disorders like Type 2 diabetes mellitus. Chronically high concentrations of circulating lipids cause a slew of problems, notably ectopic deposition of fat due to exhaustion of adipose tissue storage capacity (Schlegel, 2012). Understanding the physiology of metabolic lipids is fundamental in the effort to reverse obesity and its related pathologies. We put particular effort behind discovering new genes that control lipid transport, storage, and consumption throughout the vertebrate body.

A problem arising from high fat intake is non-alcoholic fatty liver disease (NAFLD). Worldwide, NAFLD affects 30% of adults (Gastaldelli et al., 2009). It commonly accompanies atherosclerosis (Targher et al., 2010) and a link with insulin resistance is rapidly becoming apparent (Cohen et al., 2011). The initial stage of NAFLD is hepatic steatosis, in which cytoplasmic triacylglycerol is deposited in hepatocytes. Steatosis can progress into non-alcoholic steatohepatitis (NASH), where hepatocytes begin to swell and undergo cell death, recruiting immune cells and initiating fibrosis. From here, the disease can worsen to cirrhosis, meaning the liver comprises mostly scar

tissue (collagen) and stellate cells. Finally, cirrhosis may give rise to hepatocellular carcinoma (Cohen et al., 2011).

A complete understanding of the molecular pathways underlying hepatic steatosis, and its progression into NASH, and cirrhosis remains to be established. NAFLD is approximately 39% heritable (Schwimmer et al., 2009). Several sequence variations that show correlation with hepatic steatosis in humans have been identified. One variant showing the strongest association with fatty liver occurs in PNPLA3, a triglyceride hydrolase and transacylase (Romeo et al., 2008). It is unclear how the mutation, I148M, causes an accumulation of fat in hepatocytes. Various other studies have found more susceptibility loci containing genes such as *NCAN, GCKR, LYPLAL1, APOC3,* and *PPP1R3B* (Cohen et al., 2011). Variants in these suggest several mechanisms to promote fatty liver, including down-regulation of lipases or up-regulation of fatty acid synthesis. The molecular mechanisms for how these variants contribute to hepatic lipid accumulation have not been elucidated.

Solute carrier family 16a, member 6a

Through a forward genetic screen to identify lipid storage defects, our lab previously uncovered a recessive mutation which causes hepatic steatosis, *red moon* (*rmn*). Homozygous *rmn* larvae develop this phenotype when they begin fasting, *i.e.* after the entire maternally deposited yolk lipid supply has been consumed, typically six days post-fertilization (dpf). Increased triacylglycerol in the liver relative to wild-type animals can be visualized using Oil Red O (ORO), a neutral lipid stain (**Figure 1**). With microsatellite mapping, the *rmn* locus was isolated. The mutated gene is *slc16a6a*, and

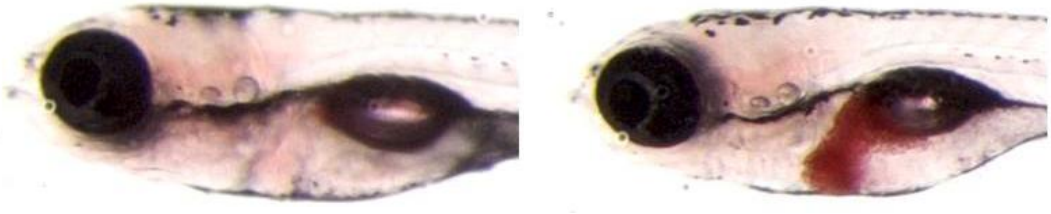

Figure 1. Whole mount staining of fixed 6dpf larve stained with Oil Red O (ORO). Note slight staining in swim bladder (surfactant lining). Provided by Amnon Schlegel.

the molecular lesion is a retro-transposable element insertion in the second exon of *slc16a6a,* which encoded an orphan plasma membrane monocarboxylate transporter (formerly MCT7). The *slc16a6a*$^{-/-}$ mutant phenotype can be rescued by ubiquitous or liver-specific re-expression of wild-type *slc16a6a*, by liver-specific expression of the human ortholog *SLC16A6,* or by re-feeding fasted animals at any time point after 6 dpf (Hugo et al., 2012).

Other MCTs have been thoroughly studied. For MCT1 through 4, the most widely characterized substrate is lactate (Halestrap, 2013a). However, new evidence has shown that MCT1 also imports ketone bodies; a causal link has been found between MCT1 deficiency and severe recurrent ketoacidosis in children (van Hasselt et al., 2014). When heterologously expressed in *Xenopus* oocytes, zebrafish Slc16a6a transported β-hydroxybutyrate across the cell membrane (Hugo et al., 2012). β-hydroxybutyrate is the major ketone body species produced during fasting (Cahill, 2006). The following model was then proposed and tested. If *slc16a6a* is mutated, then individuals are defective in releasing ketone bodies from the liver, effectively trapping ketones inside hepatocytes. The carbon atoms from liver-trapped ketone bodies in *slc16a6a*$^{-/-}$ mutant livers thus

become reincorporated into fatty acids which are stored as triacylglycerol in cytoplasmic lipid droplets (Hugo et al., 2012).

Approach for identification of new hepatic lipid metabolism genes

My goal has been to use the *slc16a6a*$^{-/-}$ mutants to find genes with which *slc16a6a* interacts by means of a modifier screen. We anticipated two types of mutants: suppressors, those with lessened hepatic steatosis, and enhancers, those with an increased hepatic steatosis (or an advanced pathological phenotype such as cirrhosis). Aside from identifying genetic interactions with *slc16a6a,* I also wanted suppressor mutations for their potential to reveal new genes that relieve steatosis. These factors, in both the suppressor and enhancer categories, could prove to be useful targets for therapeutics to combat NAFLD. To map the dominant mutations we identified, we used a whole transcriptome-based approach called Mutation Mapping Analysis Pipeline for Pooled RNA-Seq (MMAPPR) (Hill et al., 2013). The technique involves comparing wild-type and mutant whole transcriptomes (RNA-seq), searching for single nucleotide polymorphisms (SNPs) that are linked to the mutant locus. Candidate genes in the linked region can then be selected and tested directly.

Monocarboxylate transporters in cancer

In exploring publicly available clinical data pertaining to *SLC16A6*, we found a potential new disease context in which to investigate the function of this gene. Using the Oncomine interface, gene expression data show that *SLC16A6* expression is increased in melanoma (**Figure 2**). In this study, 45 primary melanomas, 18 benign melanocyte

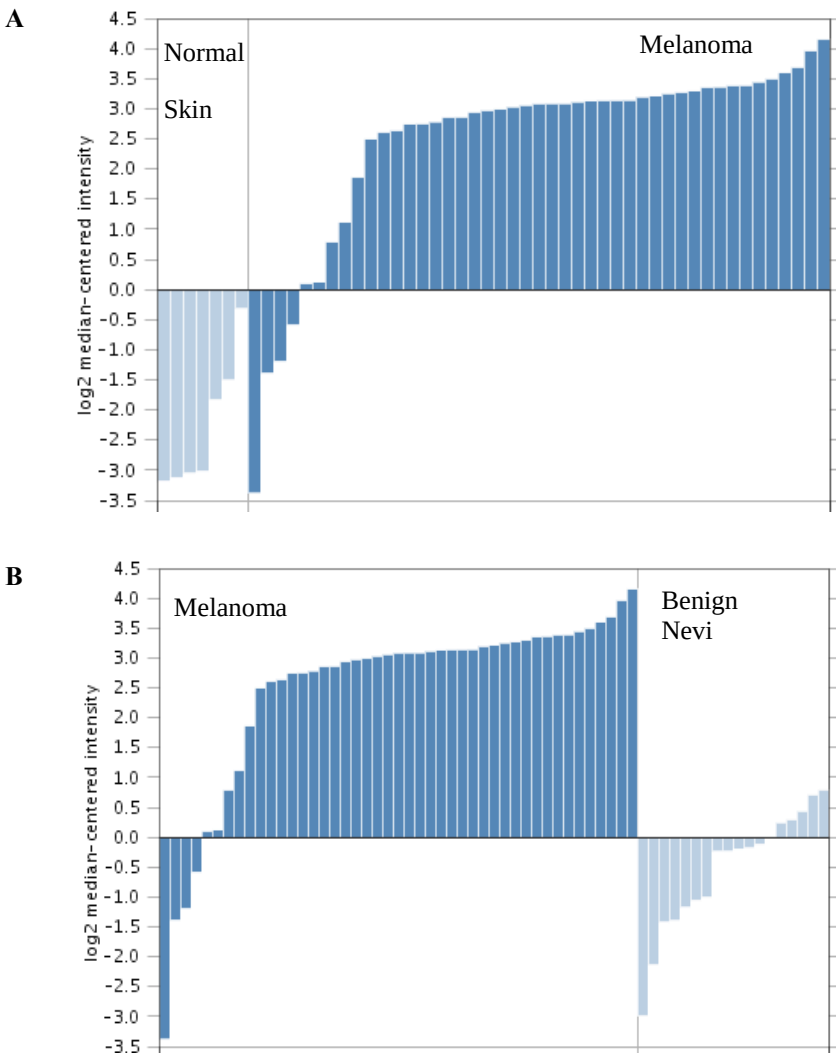

Figure 2. Affymetrix microarray of human skin samples. Oncomine query of dataset from Talantov *et al*. 2005 .Relative *SLC16A6* expression is shown in increasing order. Dark blue bars represent melanoma samples; light blue bars represent normal skin in **A** and non-cancerous melanocyte lesions in **B**. Average fold-increase in abundance in tumors compared to skin: 27.024 ($p = 6.54 \times 10^{-7}$); compared to nevi: 8.030 ($p= 3.69 \times 10^{-12}$).

lesions (nevi), and 7 normal skin tissue samples were analyzed. Compared to normal skin, *SLC16A6* levels in primary melanoma samples were approximately 27-fold higher (top 4% of overexpressed genes) and compared to benign nevi, approximately 8-fold higher (top 2% of overexpressed genes) (Talantov et al., 2005). As the pre-cancerous lesions do not have significantly increased *SLC16A6* compared with normal melanocytes, it is reasonable to hypothesize it presenting a growth advantage to lesions which enables malignancy.

Melanoma, despite affecting only 76,000 people in the US (ACS estimate for 2014), accounts for the highest portion of skin cancer deaths (Gyrylova et al., 2014). It is particularly prone to rapid growth and metastasis as skin cell turnover is extremely fast. I sought to assess whether increased SLC16A6 expression in melanoma contributes to aspects of its malignancy, including onset of tumor formation, invasion, and metastasis. Following this, I also planned to elucidate its mechanism of promoting cancerous growth.

My studies are informed by recent work placing monocarboxylate transporters as having an important role in metabolite transport for cancer cells. On a fundamental level, cancer cells rely heavily on anaerobic glycolysis for energy and synthetic substrates, which consequently generates large quantities of pyruvate and lactate. For this reason, lactate transporters of the SLC16 family are in many cases expressed at higher levels in cancerous cells than others, particularly *SLC16A1* (or *MCT1*) (Pinheiro et al., 2014; Kennedy and Dewhirst, 2010). Further, certain subpopulations of tumor cells have been shown to take up lactate as a fuel source, insinuating a symbiotic “lactate shuttling” system between subpopulations and between tumor and stroma (Kennedy and Dewhirst, 2010). It is possible that increased SLC16A6 allows melanoma cells to transport lactate

or pyruvate. However, with the evidence for β-hydryoxybutyrate transport in zebrafish, I favor a model in which ketone bodies are taken up and used by cancer cells. Ketone bodies could be advantageous to cancer cells to feed fatty acid synthesis and thus supply an increased demand for lipids (Baenke et al., 2013).

I have worked to establish a transgenic zebrafish line in with which *SLC16A6* involvement in cancer can be explored. Future experiments using this system can add another level to our current understanding of tumor metabolism. Supporting this, the human SLC16A6 protein can be studied *in vitro* to discover details about its substrate specificity and kinetics, informed by established functional conservation with zebrafish *slc16a6a.*

CHAPTER 2

total eclipse of red moon

Genetic screening for dominant modifiers of *slc16a6a*$^{-/-}$

In order to understand how liver lipid mass is controlled during fed and fasted states, a genetic screen was used to identify dominant mutations that modify the *slc16a6a*$^{-/-}$ phenotype (**Figure 3A)**. *slc16a6a*$^{-/-}$ males were mutagenized with *N*-ethyl-*N*-nitrosourea (ENU). The F_0 animals were crossed with *slc16a6a*$^{-/-}$ females, yielding F_1 families of at least 60 individuals each. Each F_1 animal was crossed to a *slc16a6a*$^{-/-}$ mate and F_2 offspring were screened for enhancement or suppression of the *slc16a6a*$^{-/-}$ phenotype. To do this, clutches of 7 dpf larvae were fixed and stained with Oil Red O (ORO) to visualize neutral lipids in livers. As I sought dominant mutations, I looked for heterozygous carriers that produced clutches in which half of the F_2 offspring show the modified phenotype and half show normal *slc16a6a*$^{-/-}$ liver staining.

I identified an F_1 individual whose offspring exhibit the appropriate pattern for carrying a dominant suppressor allele: half showed the *slc16a6a*$^{-/-}$ phenotype and half showed reduced ORO staining in the liver (**Figure 3A**: "F_2 Dominant Suppressors"). I have named this mutation *total eclipse of red moon* (*term*). I then crossed this carrier to a mapping line homozygous for the *slc16a6a*$^{-/-}$ mutation, and sorted live offspring by phenotype using Nile Red, which fluorescently stains neutral lipids yellow/green (450-

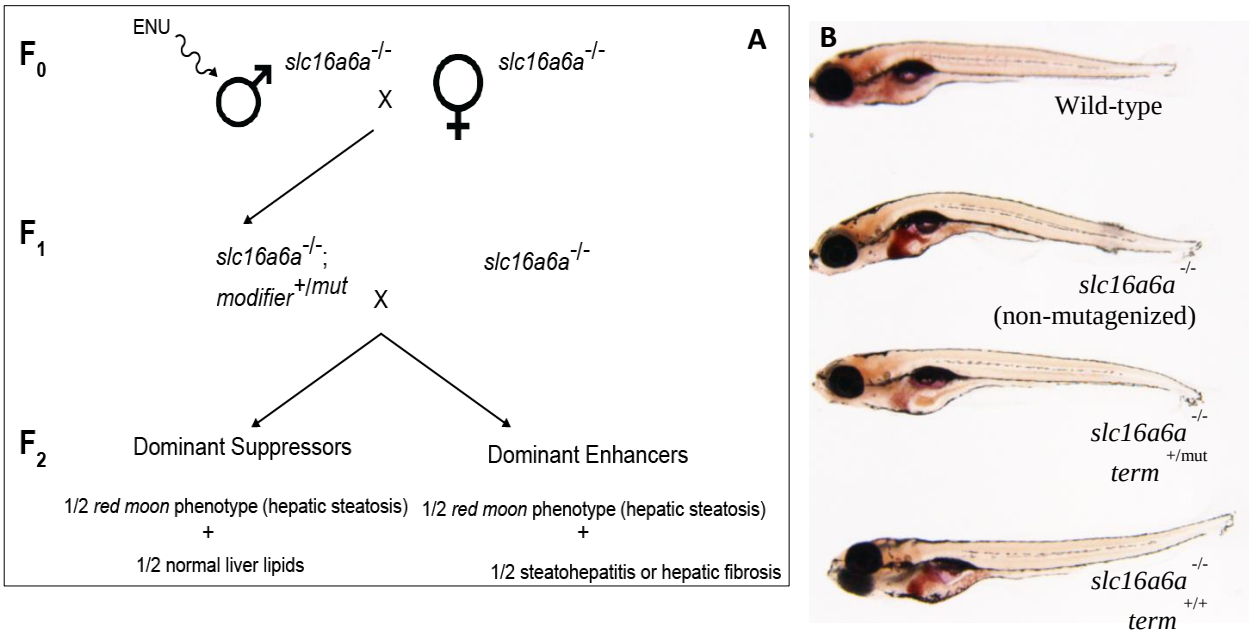

Figure 3. ***total eclipse of red moon.*** **A. *red moon* modifier screening strategy.** The red moon stock originated on an AB/Singapore genetic background. A mapping strain was generated for the F_1 outcross by crossing the *rmn* mutation into a polymorphic WIK strain. **B. Oil Red O stained *term* mutant.** 7 dpf larvae imaged under bright field light on a Leica DFC 310 FX stereo microscope.

490 nm excitation) (Fowler and Greenspan, 1985).

Mutation mapping analysis using RNA-Seq

I crossed the F_1 heterozygous *term* carrier with an individual from a mapping strain (WIK) *slc16a6a*$^{-/-}$ to create a mapping panel of F_2 individuals. After sorting as *term* carrier (+/*mut*) or non-carrier (+/+) from this clutch, the two phenotypes were split into 3 smaller pools (18 each) from which total RNA was extracted. From these samples, a cDNA library was prepared and sequenced on an Illumina HiSeq2000 next generation sequencer at the Huntsman Cancer Institute's genomic analysis core facility.

The RNA-Seq dataset from these phenotypic pools was used to map the mutation with Mutation Mapping Analysis Pipeline for Pooled RNA-Seq (MMAPPR) (Hill et al., 2013). The *term* mutation was mapped to a 5.7 megabase (Mb) region on Chromosome 7 spanning from base 16,848,097 to 22,579,615 (**Figure 4**). This peak contains a total of 115 annotated genes; see full locus via University of California Santa Cruz genome browser: http://genome.ucsc.edu/cgi-bin/hgTracks?db=danRer10&position=chr7%3A16848097-22579615&hgsid=423409963_bIyBwH3wUpAMc6RskB9pvwzLLT1r. Additionally, differential expression analysis was performed for all genes on chromosome 7, but none showed significantly different expression levels between pools (data not shown).

Candidates for the *term* gene

Unfortunately, among the SNPs detected using MMAPPR that fell in this region, we did not find one that appeared causal. I have selected four promising candidate genes to test, which are summarized in **Table 1**.

rab1ba

One *term* mutant candidate gene is *rab1ba*. In humans, Rab1b is a regulator vesicle traffic in the secretory pathway (Plutner et al., 1991). Through its interaction with Arf1, a protein also involved in vesicle assembly and suggested to act in very low density lipoprotein (VLDL) particle secretion, Rab1b may have a connection with lipoprotein particle packaging as well (Mochizuki et al., 2013). It is possible that a gain-of-function mutation in *rab1ba* could suppress hepatic lipid accumulation in the liver of *slc16a6a*$^{-/-}$

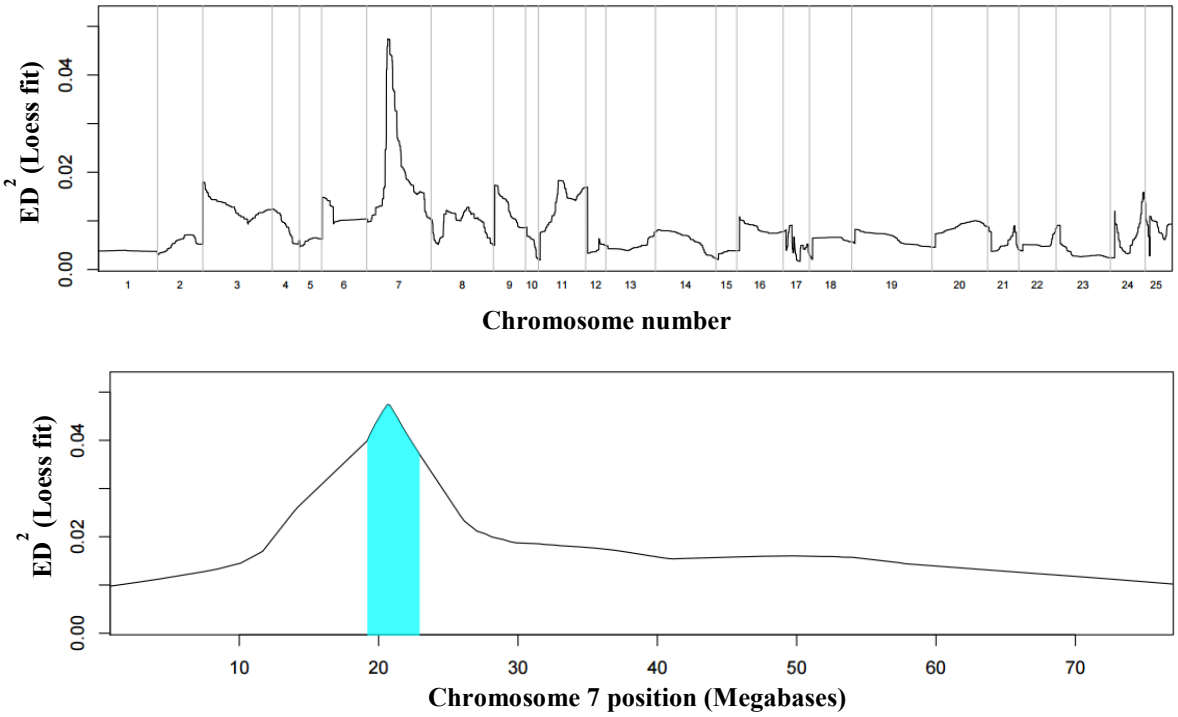

Figure 4. Single nucleotide polymorphisms segregating with *term* are clustered on chromosome 7. Throughout the assembled transcriptome, Euclidean distance scores at each nucleotide position were calculated, raised to the second power, plotted and fitted to a Loess curve. **A:** Entire transcriptome assembly, **B:** close-up of chromosome 7. SNPs in the region shaded blue (bases 16848097-22579615) were considered for candidate testing.

animals by enhancing VLDL secretion. Alternatively, a loss-of-function mutation in Rab1b, may disrupt autophagy, or cellular macromolecular recycling (Mochizuki et al., 2013), during starvation. If *rab1ba* function is diminished, fewer ketogenic amino acids will be available for ketogenesis (and subsequent diversion to neutral lipids in *slc16a6a*$^{-/-}$ livers).

Table 1: Candidate genes in the term-linked region. Genome positions based on GRCz10 assembly. Protein function inferred by homology with human ortholog.

Gene position (base on Chr. 7)	**Gene symbol and name**	**Protein function**	**Hypothetical mechanism of dominant *red moon* suppression**
17,848,643-17,864,127	*rab1ba* RAS oncogene family A	GTPase essential for vesicle formation in early secretory pathway	Gain of function enhances VLDL secretion, allowing triacylglycerol export
19,310,089-19,335,574	*slc7a7* solute carrier family 7	Light chain of large neutral amino acid transport complex y^+L	Dominant negative or haploinsufficient phenotypes impair import of amino acid substrates for ketogenesis
19,779,204-19,802,360	*slc16a13* solute carrier family 16	Monocarboxylic acid transporter	Gain of function phenotype compensates for loss of *slc16a6a*
20,272,125-20,278,479	*slc3a2a* solute carrier family 3	Heavy chain of large neutral amino acid transport complex y^+L	Dominant negative or haploinsufficient phenotypes impair import of amino acid substrates for ketogenesis

slc7a7

The human ortholog *SLC7A7* encodes the light chain of the y+L system, a protein essential for intracellular amino acid transport as a subunit of LAT1 (SLC3A2), the large neutral amino acid transport complex in the plasma membrane (Moger et al., 2012). Loss of function mutations in human *SLC7A7* cause lysinuric protein intolerance (Borsani et al., 1999). Lysine is a ketogenic amino acid (Cahill, 2006).

slc3a2a

Human *SLC3A2* is the heavy chain of the y+L system, comprising SLC7A7 and SLC3A2. Disruption of *slc3a2* would make sense in the context of the *term* phenotype for the same reason as its counterpart slc7a7 would. A caveat to this hypothesis is that zebrafish *in situ* experiments has only found expression in the nervous system, pancreas, and yolk syncytial layer of early-stage embryos (Moger et al., 2012), while Human data indicates that the ortholog, Slc3a2, is expressed in the human liver (MOPED and PaxDb). However, this does not rule out cell-non-autonomous effects of a mutated *slc3a2*.

slc16a13

This gene was our strongest candidate, as it is encodes an orphan monocarboxylate transporter. The most obvious hypothesis for how mutations in *slc16a13* suppress hepatic steatosis in *slc16a6a*$^{-/-}$ animals is a gain-of-function scenrario, in which Slc16a13 exports β-hydroxybutyrate. Interestingly, SNPs in the *SLC16A13* locus (which includes the neighboring orphan MCT gene *SLC16A11*) were identified in two separate genome-wide association studies (GWAS) as conferring risk to the development of Type 2 Diabetes Mellitus (Hara et al., 2014; Williams et al., 2014).

Results

I cloned *slc16a13* and *rab1ba* cDNAs from *term* mutants. Upon Sanger sequencing, no coding differences were observed when compared with non-carriers (not shown). The other two candidate cDNAs will be cloned and additional candidates may be selected.

Materials and methods

Mutagenesis and screening

slc16a6a$^{-/-}$ adult males were exposed to *N*-ethyl-*N*-nitrosourea (ENU). These were each out-crossed to a *slc16a6a*$^{-/-}$ female, the offspring of which were raised and subsequently outcrossed again to a *slc16a6a*$^{-/-}$ mate (see Figure 3A). These F_2 individuals were screened for liver steatosis by fixing in 4% formaldehyde at 7 dpf (≥1 hr), staining with Oil Red O (1 hr, shaking), and rehydrating in phosphate buffered saline (PBS). Images of F_2 individuals were taken under bright field illumination on a Leica DFC 310 FX stereo microscope after mounting the fixed and ORO-stained larvae in 1% low melt agarose.

Live phenotype sorting

Live F_2 offspring of term$^{+/mut}$ x WIK *slc16a6a*$^{-/-}$ were sorted at 7 dpf using Nile Red stain. Larvae were incubated in 0.5 μg/mL Nile Red for 30 min in the dark and anaesthetized with tricaine. Larvae were observed under fluorescence on a Leica DFC 310 FX stereo microscope using GFP range excitation (450-490 nm) and sorted according to intensity of yellow liver staining (with WIK *slc16a6a*$^{-/-}$ and WIK *slc16a6a*$^{+/+}$ from non-mutagenized parents for reference).

RNA-Seq sample preparation and MMAPPR

After Nile Red sorting, three pools (n=18) of each phenotype were collected and homogenized. Total RNA was isolated from the homogenates using the RNeasy RNA extraction kit (Qiagen). Samples were submitted to the University of Utah genomics core

facility, where a cDNA library was generated and sequenced with an Illumina Hi-Seq 2500 instrument (described in the following two subsections). *In silico* analysis on RNA-Seq data using MMAPPR software was performed by Jonathon Hill of the Joseph Yost laboratory at the University of Utah as described in (Hill et al., 2013). Library construction was performed using the Illumina TruSeq RNA Sample Preparation Kit v2 (RS-122-2001 and RS-122-2002) as described in the next two subsections taken from the Univeristy of Utah's High Throughput Genomics Core Facility web-based system named GNomEx (https://hci-bio-app.hci.utah.edu/gnomex).

Library construction

Briefly, total RNA (100 ng to 4 ug) is poly-A selected using poly-T oligo-attached magnetic beads. Poly-A RNA is eluted from the magnetic beads, fragmented and primed with random hexamers in preparation for cDNA synthesis. First strand reverse transcription is accomplished using Superscript II Reverse Transcriptase (Invitrogen cat#18064-014). Following second strand synthesis, the cDNA is converted to blunt-ended fragments with 5'-phosphates and 3'-hydroxyl groups using a combination of enzymes that perform fill-in reactions and exhibit exonuclease activity. An A-base is added to the blunt ends as a means to prepare the fragments for adapter ligation and block concatamer formation during the ligation step. Adapters containing a T-base overhang are ligated to the A-tailed DNA fragments. Ligated fragments are PCR-amplified (12 cycles) and the amplified library is purified by Agencourt AMPure XP beads (Beckman Coulter Genomics cat#A63881). The concentration of the amplified library is measured with a NanoDrop spectrophotometer and an aliquot of the library is resolved on an

Agilent 2200 Tape Station using a D1K (cat# 5067-5361 and 5067-5362) or a High Sensitivity D1K (cat# 5067-5363 and 5067-5364) assay to define the size distribution of the sequencing library. Libraries are adjusted to a concentration of approximately 10 nM and quantitative PCR is performed using the KapaBiosystems Kapa Library Quant Kit (cat# KK4824) to calculate the molarity of adapter ligated library molecules. The concentration is further adjusted following qPCR to prepare the library for Illumina sequence analysis.

Sequencing

Sequencing libraries (18 pM) were chemically denatured and applied to an Illumina TruSeq v3 single read flowcell using an Illumina cBot. Hybridized molecules were clonally amplified and annealed to sequencing primers with reagents from an Illumina TruSeq SR Cluster Kit v3-cBot-HS (GD-401-3001). Following transfer of the flowcell to an Illumina HiSeq instrument (HCS v2.0.12 and RTA v1.17.21.3), a 50 cycle single read sequence run was performed using TruSeq SBS v3 sequencing reagents (FC-401-3002).

Cloning candidate genes

Pooled *term*$^{+/mut}$ and *term*$^{+/+}$ RNA samples were reverse transcribed, providing a template for polymerase chain reaction (PCR) amplification of candidate genes. These two steps were achieved with a SuperScriptIII/Platinum Taq combination RT-PCR kit (Invitrogen/Life Technologies). Products were electrophoresed in a 1% agarose gel, excised, and purified using a Gel extraction kit from Bioneer. The products were ligated

into a linearized pGEM®-T Easy Vector (Promega) with T4 DNA ligase (Promega) and the resulting plasmids were transformed into NEB-10β competent cells (New England Biolabs). These were plated on LB agar plates with ampicillin, x-gal, and IPTG for blue/white selection of colonies containing successful recombinants. Plasmids were isolated from white colonies and submitted for Sanger Sequencing at the University of Utah Sequencing core facility with primers T7 and SP6. A list of all primer sequences and PCR programs can be found in the **Appendix**.

CHAPTER 3

TRANSGENIC EXPRESSION OF HUMAN SLC16A6

Human SLC16A6 in mammalian cells

In order to characterize human SLC16A6, I first turned to stable transfection into mammalian cells to achieve protein expression, with the help of Nicola Longo and colleagues. I transfected a plasmid encoding a SLC16A6-EGFP fusion construct into Chinese hamster ovary (CHO) cells, hoping to obtain clones with green fluorescent plasma membranes (**Figure 5A**). When visualized with confocal microscopy, however, both empty pEGFP-N1 vector and SLC16A6-EGFP transfected cells showed diffuse cytoplasmic green fluorescence (**Figure 5B**). The fusion protein may not have been targeted correctly to the plasma membrane.

Transgenic SLC16A6 zebrafish

Next, I generated a transgenic construct to express SLC16A6 without a large epitope tag that might interfere with trafficking (**Figure 6A)**. Using the promoter from the liver-specific gene *fabp10a* to drive its expression, I generated a transgenic construct with *SLC16A6* preceded by the zebrafish consensus Kozak sequence and enhanced green fluorescent protein (EGFP) on the C-terminus: *Tg*(*fabp10:SLC16A6,EGFP*). A viral 2A peptide coding sequence was placed between the *SLC16A6* and *EGFP* sequences to

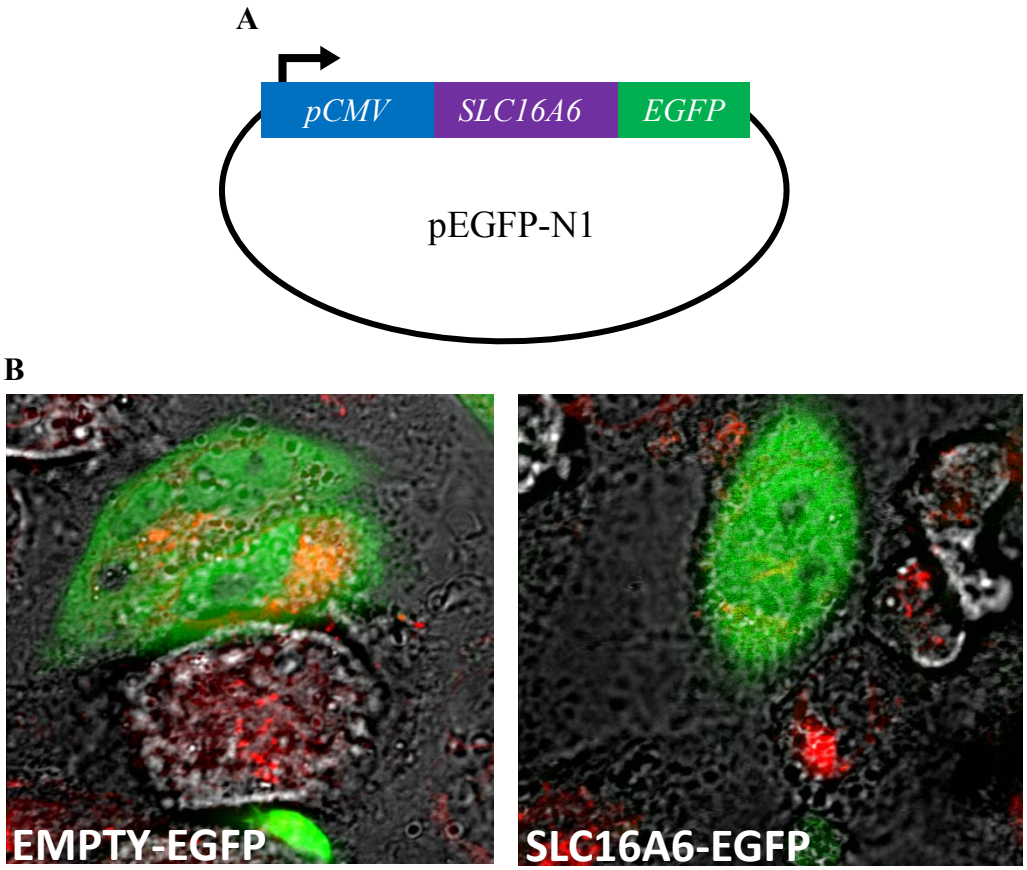

Figure 5. A. Strategy for transgenic expression of human SLC16A6 in mammalian cells. A. Mammalian over-expression construct for SLC16A6 **B.** From Xue Yin, Nicola Longo Lab: cultured CHO cells transfected with EGFP-tagged SLC16A6 in cultured. Confocal images, golgi labeled red with BODIPY-ceramide.

liberate the EGFP protein from SLC16A6: during translation, ribosomes fail to make a peptide bond between proline and glycine in the 2A sequence, effectively "cleaving" the nascent polypeptide (Diao and White, 2012). This strategy allows expression of a marker for translation of *SLC16A6* without the complication of a large protein tag.

Upon injection of this construct into one cell *slc16a6a*$^{-/-}$ embryos and upon screening for EGFP, mosaic expression of EGFP in the liver was evident (**Figure 6B).** Note that the yellow fluorescence in the intestine and gallbladder is due to bile. To assess

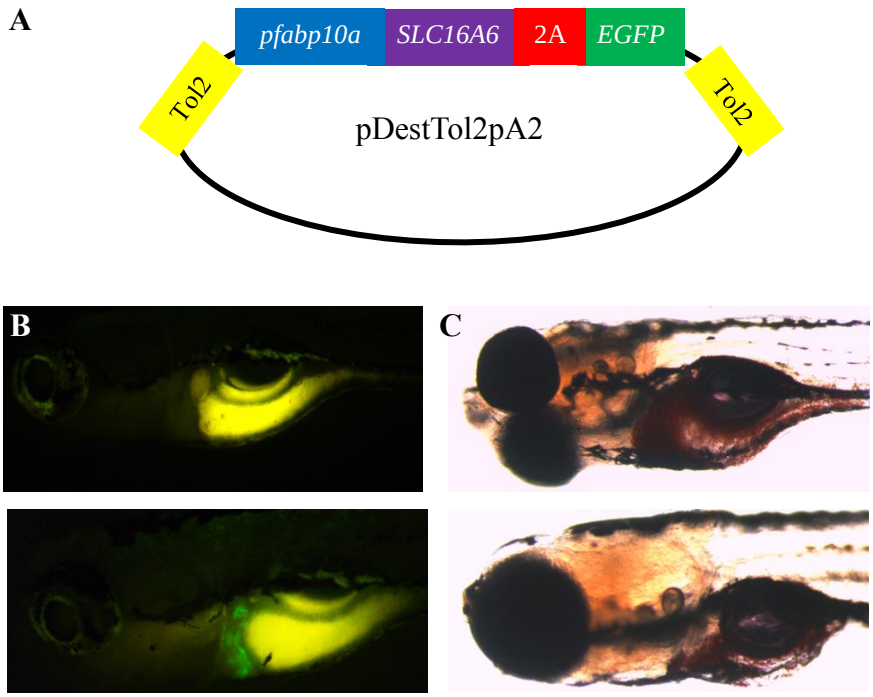

<u>Figure 6</u>: Transgenic expression of SLC16A6 in zebrafish liver A. Schematic representation of Tol2 destination vector containing the transposable cassette *fabp10:SLC16A6,EGFP*. **B.** 7 dpf *slc16a6a*$^{-/-}$ larvae injected with the *fabp10:SLC16A6,EGFP*. Top: uninjected, bottom: injected with transgenic construct. Images taken on a Leica DFC 310 FX Stereo microscope using GFP range excitation (450-490 nm). Yellow autofluorescence is due to fats in gut lumen and gallbladder. **C**. Oil Red O-stained 7 dpf larvae. Top: uninjected, Bottom: injected with the transgenic construct.

whether SLC16A6 was expressed and functional, I injected the *Tg*(*fabp10:SLC16A6,EGFP*) construct into *slc16a6a*$^{-/-}$ embryos and determined that hepatic steatosis had been rescued (**Figure 6C**). Note that this rescue is partial, as the transgene is mosaically expressed: the ORO staining is limited to ventral portions of the liver. I have also attempted to see SLC16A6 by immunodetection in these green-livered larvae (western blot remains to be optimized).

Future directions

Melanoma studies with SLC16A6

The *SLC16A6,EGFP* cassette will be subcloned into miniCoopR and the resulting plasmid can be used to study modifiers of melanomagenesis when injected into zebrafish (Ceol et al., 2011). This transgenic reagent will be injected into wild-type and *slc16a6a*$^{-/-}$ mutants.

The melanoma fish line contains one transgene (*mitfa:BRAF*$^{V600E/V600E}$) and two homozygous null mutations (*p53*$^{-/-}$ and *mitfa*$^{-/-}$). The human *BRAF* transgene, driven by the promoter of melanocyte-specific *mitfa*, reflects the most common mutation linked to melanoma, which causes excessive activity of the mitogen-activated protein kinase kinase (MAPKK) *BRAF*. As an additional insult to observe rapid development and progression of melanoma, this is done in a *p53* null background. Additionally, deletion of *mitfa* prevents melanin biosynthesis (Ceol et al., 2011). This mutation is present so that additional genes may be introduced on a miniCoopR construct carrying functional *mitfa*, so that the coincidence of pigment production rescue and expression of the transgene of interest can be achieved in a cell-autonomous manner (**Figure 7)**.

With my successfully expressing *SLC16A6* construct, the cDNA can be subcloned into miniCoopR and introduced into Tg(*mitfa:BRAF*$^{V600E/V600E}$) *p53*$^{-/-}$ *mitfa*$^{-/-}$ *slc16a6a*$^{-/-}$ embryos. From the microarray data (Talantov et al., 2005), it seems likely that transgenic expression of *SLC16A6* will be advantageous to melanoma tissue. Survival, tumor onset, growth, and metastasis can be measured as described previously (Ceol, 2011). Compared to control animals, I expect accelerated tumor incidence and/or growth and a subsequently reduced survival time in animals overexpressing *SLC16A6*. As the

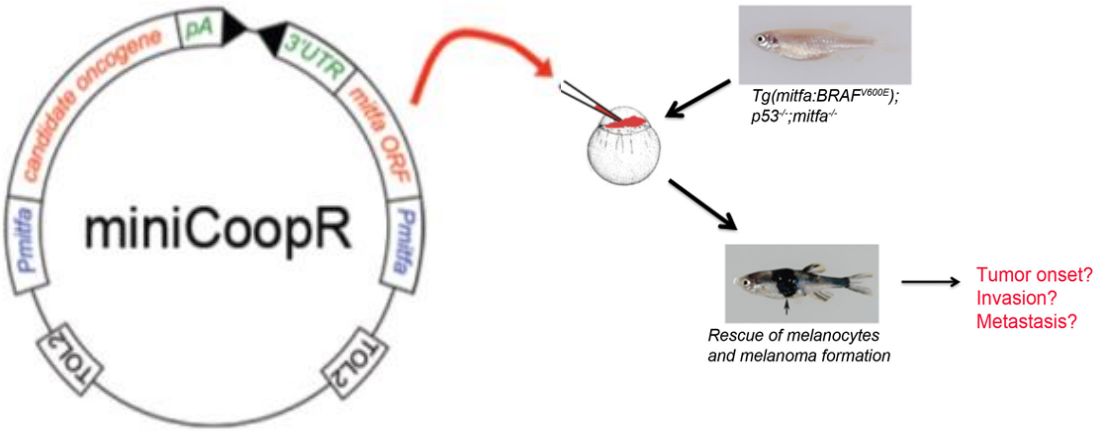

Figure 7. Transgenesis strategy to test *SLC16A6* involvement in melanoma. A "candidate oncogene" (*SLC16A6* in my case) can be put under the control of the *mitfa* promoter in tandem with a functional *mitfa* cDNA. The two gene cassettes are between transposition sites, allowing their genomic insertion when the plasmid is injected into one-cell embryos with Tol2 transposase. In Tg(*mitfa:BRAF*$^{V600E/V600E}$) *p53*$^{-/-}$ *mitfa*$^{-/-}$ animals, melanocytes expressing this construct will regain the capacity for melanin production. Once mature, survival, time of tumor onset, and metastasis can be assayed. Adapted from Ceol *et al. 2011* supplementary materials.

microarray analysis had no information regarding whether samples belonged to metastatic tumors, the question of whether *SLC16A6* promotes metastasis remains unpredictable.

If *SLC16A6* does enhance the aforementioned cancer phenotypes, this experiment will also tell us whether the effects are cell-autonomous. If only the melanin-producing populations of melanocytes worsen upon *SLC16A6* introduction, then the gene only benefits tumor tissue in which it is expressed. If both pigmented and un-pigmented tumors increase in incidence, growth, or metastasis, then *SLC16A6* expression is promoting a cancerous environment on a more global scale.

Biochemical characterization of human SLC16A6

Because human *SLC16A6* functionally rescues *slc16a6a*$^{-/-}$ animals, we are interested in characterizing the human protein and exploring further roles in human disease. We hope to successfully express this cassette in mammalian cells in order to identify substrates and determine kinetic parameters for SLC16A6 transport. I hypothesize that, as with Slc16a6a, the human protein also shows a preference for β-hydroxybutrate. On a nonquantitative level, voltage clamp experiments can be done to determine whether incubation with β-hydroxybutyrate incubation generates an inward current in *Xenopus* oocytes expressing human SLC16A6 (Hugo et al., 2012). Further, mammalian cells expressing SLC16A6 can be assayed for the rate at which they take up a variety of MCT substrates. This can be done in collaboration with Nicola Longo, using his established cluster tray method for testing cationic transport substrates (Ardon et al., 2010; Scaglia et al., 1999). B-hydroxybutyrate can be detected by an enzymatic assay using 3-hydroxybutyrate dehydrogenase, whose catalysis produces NADH which can be measured with a colorimetric probe (Cayman Chemicals). From time course experiments, kinetic parameters can be determined according to a Michaelis-Menten model (Scaglia et al., 1999). An important note regarding substrate specificity is that β-hydroxybutyrate accounts for 75% of circulating ketone bodies while acetoacetate makes up the remainder. Thus, acetoacetate transport should also be measured, though no simple detection assay is currently available. It may be advantageous to cancer cells to pump out lactate or pyruvate, so these should be tested as well. The outcome of these experiments could provide additional insights into melanoma tumor metabolism. Cancer cells in general suppress oxidative phosphorylation and fatty acid oxidation which could justify a

need for partially oxidized substrates (*i.e.* ketone bodies). Alternatively, it is likely that SLC16A6 transports lactate, which may be an advantage for proliferating tumor cells, which produce an excess of lactate from glycolysis due to minimal mitochondrial oxidation (Draoui and Feron, 2011).

Materials and methods

SLC16A6 transgensis in mammalian cell culture

SLC16A6 cDNA was amplified off of a plasmid already containing *SLC16A6* named "pME-HuSLC" made by Lourdes Cruz-García in 2011 (Hugo et al., 2012) using primers "HsSLC-F_Xho" and "HsSLCnostop-R" containing sites for XhoI and SacII restriction endonucleases, respectively. The resultant PCR product and pEGFP-N1 vector (Clontech) were digested with Xho I and SacII (New England Biolabs). The vector digestion product was dephosphorylated using Calf Intestinal Alkaline Phosphatase (Promega). The insert and vector (3:1 molar ratio) were ligated together with T4 DNA ligase (Promega), and transformed into NEB 10β competent cells (New England Biolabs). Plasmids (pEGFP-N1-SLC16A6) were isolated from bacterial clones and the presence of the insert was verified by Sanger sequencing using primers "seq_pEGFPN1-F" and "seq_pEGFPN1-R".

The following was done by Xue Yin of Nicola Longo's laboratory at the University of Utah. Each plasmid, pEGFP-N1-SLC16A6 and empty pEFGP-N1 vector, was transfected into Chinese Hampster Ovary (CHO) cells using lipofectamine. Selection for stable clones with integrated *SLC16A6* cassette was performed using neomycin. Clones were screened for the presence of GFP with fluorescence microscopy.

Transgenic zebrafish expressing SLC16A6

This expression plasmid was constructed using a standard Gateway cloning strategy with materials from Invitrogen/Life Technologies. Specific for zebrafish transgenesis is the "Tol2 kit" developed by Kwan and colleagues (Kwan et al., 2007). I amplified *SLC16A6* using primers "attB1-SLC16A6 zebrafish kozak" and "attB2R-SLC16A6 C-term 2AEGFP" off of pME-HuSLC. The resultant PCR product excludes the stop codon and includes the zebrafish consensus Kozak sequence (GCAACC) immediately upstream of the start codon. This PCR product was electrophoresed on a 1% agarose gel, excised using a gel extraction kit (Bioneer), then recombined into pDONR-221 with BP clonase (Invitrogen/Life Technologies) to generate pME-zSLC16A6. Clones were sequenced with M13F and M13R to verify presence of insert. pME-zSLC16A6 was recombined with p5E-fabp10a (Lourdes Cruz-García, University of Portsmouth) and p3E-2AEGFP (Kristen Kwan, University of Utah) into pDestTol2pA2 using LR clonase (Invitrogen/Life Technologies). The combined insert of the final destination vector (**Figure 6A**) was sequenced using primers seq_pDestTol2pA2_B4, seq_fabp10a_B1, seq_SLC16A6nostop_B2, seq_2AeGFP_B3.

The transgenic construct was combined with Tol2 transposase capped and tailed mRNA as described previously (Kwan et al., 2007). This cocktail was injected into one-cell *slc16a6a*$^{-/-}$ embryos. Embryos were raised to 7 dpf and then screened for hepatic GFP expression under fluorescence on a Leica DFC 310 FX stereo microscope using GFP range excitation (450-490 nm). Individuals showing hepatic GFP expression were mounted in 1% low melting point agarose for imaging. Larvae were either imaged under

fluorescent light or fixed in formaldehyde, stained with ORO (as described in the above methods section), and imaged under bright field light.

APPENDIX

PCR PRIMERS AND PARAMETERS

RT-PCR amplification of *term* candidate genes

rab1ba 5UTR 2	TCAAGTGACTGGATCCAACG
rab1ba 3UTR 2	GGACTTTACGTACAGGGGGC

Program:	Temp (°C)	Time (min:sec)
cDNA synthesis	55	30:00
Initial Denaturation	94	02:00
Denaturation	94	00:15
Annealing	60	00:30
Extension	68	01:00
Repeat steps 3-5 x 45		
Final extension	68	05:00

slc16a13 5'UTR 2	GAACCTTCCGCACGTGTAGT
slc16a13 3'UTR 2	TGCTGCTTTTGAAACTCCAA

Program:	Temp (°C)	Time (min:sec)
cDNA synthesis	55	30:00
Initial Denaturation	94	02:00
Denaturation	94	00:15
Annealing	60	00:30
Extension	68	02:00
Repeat steps 3-5 x 45		
Final extension	68	05:00

Primers for SLC16A6 amplification for expression in CHO cells

HsSLC-F_Xho	ggggccctcgaggCAGGCTATGACCCAAAA
HsSLCnostop-R	agagagccacggTACCGGCTCCATTTGC

Program:	Temp (°C)	Time (min:sec)
Initial Denaturation	95	02:00
Denaturation	95	00:30
Annealing	53	00:30
Extension	72	01:30
Repeat step 2-5 x 30		
Final extension	72	05:00

Primers for SLC16A6 amplification for expression in zebrafish

attB1-SLC16A6 zebrafish Kozak
GGGGACAAGTTTGTACAAAAAAGCAGGCTgcaaccATGACCCA
attB2R-SLC16A6 C-term 2AEGFP
GGGGACCACTTTGTACAAGAAAGCTGGGTaTACCGGCT

Program:	Temp (°C)	Time (min:sec)
Initial Denaturation	98	01:00
Denaturation	98	00:10
Annealing	55	00:15
Extension	72	00:50
Repeat steps 2-4 x 30		
Final extension	72	05:00

Sanger sequencing primers

T7	TAATACGACTCACTATAGGG
SP6	ATTTAGGTGACACTATAG
seq_pEGFPN1-F	CATGGTCCTGCTGGAGTTCGTG
seq_pEGFPN1-R	CCTCTACAAATGTGGTATGGCTG
M13F	TGTAAAACGACGGCCAGT
M13R	CAGGAAACAGCTATGACCATG
seq_pDestTol2pA2_B4	GGCAGCAGTGCAATTCTAACAG
seq_fabp10a_B1	GGTCATTGACTGAACTCCTCT
seq_SLC16A6nostop_B2	CAAAGGTAGTGAGCCATCGT
seq_2AEGFP_B3	GAGGCGCGCCTCTAGAACTAT

REFERENCES

Ardon, O., C. Amat di San Filippo, G.S. Salomons, and N. Longo. 2010. Creatine transporter deficiency in two half-brothers. *Am. J. Med. Genet. A.* 152A:1979–83. doi:10.1002/ajmg.a.33551.

Baenke, F., B. Peck, H. Miess, and A. Schulze. 2013. Hooked on fat: the role of lipid synthesis in cancer metabolism and tumour development. *Dis. Model. Mech.* 6:1353–63. doi:10.1242/dmm.011338.

Borsani, G., M.T. Bassi, M.P. Sperandeo, A. De Grandi, A. Buoninconti, M. Riboni, M. Manzoni, B. Incerti, A. Pepe, G. Andria, A. Ballabio, and G. Sebastio. 1999. SLC7A7, encoding a putative permease-related protein, is mutated in patients with lysinuric protein intolerance. *Nat. Genet.* 21:297–301.

Cahill, G.F. 2006. Fuel metabolism in starvation. *Annu. Rev. Nutr.* 26:1–22. doi:10.1146/annurev.nutr.26.061505.111258.

Ceol, C.J. 2011. supplementary materials.

Ceol, C.J., Y. Houvras, J. Jane-Valbuena, S. Bilodeau, D. a Orlando, V. Battisti, L. Fritsch, W.M. Lin, T.J. Hollmann, F. Ferré, C. Bourque, C.J. Burke, L. Turner, A. Uong, L. a Johnson, R. Beroukhim, C.H. Mermel, M. Loda, S. Ait-Si-Ali, L. a Garraway, R. a Young, and L.I. Zon. 2011. The histone methyltransferase SETDB1 is recurrently amplified in melanoma and accelerates its onset. *Nature*. 471:513–7. doi:10.1038/nature09806.

Cohen, J.C., J.D. Horton, and H.H. Hobbs. 2011. Human fatty liver disease: old questions and new insights. *Science*. 332:1519–23. doi:10.1126/science.1204265.

Diao, F., and B.H. White. 2012. A novel approach for directing transgene expression in Drosophila: T2A-Gal4 in-frame fusion. *Genetics*. 190:1139–44. doi:10.1534/genetics.111.136291.

Draoui, N., and O. Feron. 2011. Lactate shuttles at a glance: from physiological paradigms to anti-cancer treatments. *Dis. Model. Mech.* 4:727–32. doi:10.1242/dmm.007724.

Fowler, S.D., and P. Greenspan. 1985. Application of Nile red, a fluorescent hydrophobic probe, for the detection of neutral lipid deposits in tissue sections: comparison with oil red O. *J. Histochem. Cytochem.* 33:833–836. doi:10.1177/33.8.4020099.

Gastaldelli, A., M. Kozakova, K. Højlund, A. Flyvbjerg, A. Favuzzi, A. Mitrakou, and B. Balkau. 2009. Fatty liver is associated with insulin resistance, risk of coronary heart disease, and early atherosclerosis in a large European population. *Hepatology*. 49:1537–44. doi:10.1002/hep.22845.

Gyrylova, S.N., M.B. Aksenenko, D.V. Gavrilyuk, N.V. Palkina, Y.A. Dyhno, T.G. Ruksha, and I.P. Artyukhov. 2014. Melanoma Incidence Mortality Rates and Clinico-Pathological Types in the Siberian Area of the Russian Federation. *Asian Pacific J. Cancer Prev.* 15:2201–2204. doi:10.7314/APJCP.2014.15.5.2201.

Halestrap, A.P. 2013a. The SLC16 gene family - structure, role and regulation in health and disease. *Mol. Aspects Med.* 34:337–49. doi:10.1016/j.mam.2012.05.003.

Halestrap, A.P. 2013b. Monocarboxylic acid transport. *Compr. Physiol.* 3:1611–43. doi:10.1002/cphy.c130008.

Hara, K., H. Fujita, T. a Johnson, T. Yamauchi, K. Yasuda, M. Horikoshi, C. Peng, C. Hu, R.C.W. Ma, M. Imamura, M. Iwata, T. Tsunoda, T. Morizono, N. Shojima, W.Y. So, T.F. Leung, P. Kwan, R. Zhang, J. Wang, W. Yu, H. Maegawa, H. Hirose, K. Kaku, C. Ito, H. Watada, Y. Tanaka, K. Tobe, A. Kashiwagi, R. Kawamori, W. Jia, J.C.N. Chan, Y.Y. Teo, T.E. Shyong, N. Kamatani, M. Kubo, S. Maeda, and T. Kadowaki. 2014. Genome-wide association study identifies three novel loci for type 2 diabetes. *Hum. Mol. Genet.* 23:239–46. doi:10.1093/hmg/ddt399.

Van Hasselt, P.M., S. Ferdinandusse, G.R. Monroe, J.P.N. Ruiter, M. Turkenburg, M.J. Geerlings, K. Duran, M. Harakalova, B. van der Zwaag, A. a Monavari, I. Okur, M.J. Sharrard, M. Cleary, N. O'Connell, V. Walker, M.E. Rubio-Gozalbo, M.C. de Vries, G. Visser, R.H.J. Houwen, J.J. van der Smagt, N.M. Verhoeven-Duif, R.J. a Wanders, and G. van Haaften. 2014. Monocarboxylate transporter 1 deficiency and ketone utilization. *N. Engl. J. Med.* 371:1900–7. doi:10.1056/NEJMoa1407778.

Hill, J.T., B.L. Demarest, B.W. Bisgrove, B. Gorsi, Y.-C. Su, and H.J. Yost. 2013. MMAPPR: mutation mapping analysis pipeline for pooled RNA-seq. *Genome Res.* 23:687–97. doi:10.1101/gr.146936.112.

Hugo, S.E., L. Cruz-Garcia, S. Karanth, R.M. Anderson, D.Y.R. Stainier, and A. Schlegel. 2012. A monocarboxylate transporter required for hepatocyte secretion of ketone bodies during fasting. *Genes Dev.* 26:282–293. doi:10.1101/gad.180968.111.

Kennedy, K.M., and M.W. Dewhirst. 2010. Tumor metabolism of lactate: the influence and therapeutic potential for MCT and CD147 regulation. *Futur. Oncol.* 6:1–32. doi:10.2217/fon.09.145.Tumor.

Kwan, K.M., E. Fujimoto, C. Grabher, B.D. Mangum, M.E. Hardy, D.S. Campbell, J.M. Parant, H.J. Yost, J.P. Kanki, and C.-B. Chien. 2007. The Tol2kit: a multisite

gateway-based construction kit for Tol2 transposon transgenesis constructs. *Dev. Dyn.* 236:3088–99. doi:10.1002/dvdy.21343.

Mochizuki, Y., R. Ohashi, T. Kawamura, H. Iwanari, T. Kodama, M. Naito, and T. Hamakubo. 2013. Phosphatidylinositol 3-phosphatase myotubularin-related protein 6 (MTMR6) is regulated by small GTPase Rab1B in the early secretory and autophagic pathways. *J. Biol. Chem.* 288:1009–21. doi:10.1074/jbc.M112.395087.

Moger, J., S. Faroq, E. Cartwright, I.B. Dawid, S.W. Wilson, T. Kudoh, A. Takesono, and S. Farooq. 2012. Solute carrier family 3 member 2 (Slc3a2) controls yolk syncytial layer (YSL) formation by regulating microtubule networks in the zebrafish embryo. *Proc. Natl. Acad. Sci.* 109:5548–5548. doi:10.1073/pnas.1203335109.

Pinheiro, C., V. Penna, F. Morais-Santos, L.F. Abrahão-Machado, G. Ribeiro, E.C. Curcelli, M. V Olivieri, S. Morini, I. Valença, D. Ribeiro, F.C. Schmitt, R.M. Reis, and F. Baltazar. 2014. Characterization of monocarboxylate transporters (MCTs) expression in soft tissue sarcomas: distinct prognostic impact of MCT1 sub-cellular localization. *J. Transl. Med.* 12:118. doi:10.1186/1479-5876-12-118.

Plutner, H., A.D. Cox, S. Pind, R. Khosravi-far, J.R. Bourne, R. Schwaninger, C.J. Der, and W.E. Balch. 1991. Rablb Regulates Vesicular Transport between the Endoplasmic Reticulum and Successive Golgi Compartments. 115:31–43.

Romeo, S., J. Kozlitina, C. Xing, A. Pertsemlidis, D. Cox, L. a Pennacchio, E. Boerwinkle, J.C. Cohen, and H.H. Hobbs. 2008. Genetic variation in PNPLA3 confers susceptibility to nonalcoholic fatty liver disease. *Nat. Genet.* 40:1461–5. doi:10.1038/ng.257.

Scaglia, F., Y. Wang, and N. Longo. 1999. Functional characterization of the carnitine transporter defective in primary carnitine deficiency. *Arch. Biochem. Biophys.* 364:99–106. doi:10.1006/abbi.1999.1118.

Schlegel, A. 2012. Studying non-alcoholic fatty liver disease with zebrafish: a confluence of optics, genetics, and physiology. *Cell. Mol. Life Sci.* 69:3953–3961. doi:10.1007/s00018-012-1037-y.

Schwimmer, J.B., M. a Celedon, J.E. Lavine, R. Salem, N. Campbell, N.J. Schork, M. Shiehmorteza, T. Yokoo, A. Chavez, M.S. Middleton, and C.B. Sirlin. 2009. Heritability of nonalcoholic fatty liver disease. *Gastroenterology*. 136:1585–92. doi:10.1053/j.gastro.2009.01.050.

Talantov, D., A. Mazumder, J.X. Yu, T. Briggs, Y. Jiang, J. Backus, D. Atkins, and Y. Wang. 2005. Novel genes associated with malignant melanoma but not benign melanocytic lesions. *Clin. Cancer Res.* 11:7234–42. doi:10.1158/1078-0432.CCR-05-0683.

Targher, G., C.P. Day, and E. Bonora. 2010. Risk of cardiovascular disease in patients with nonalcoholic fatty liver disease. *N. Engl. J. Med.* 363:1341–50. doi:10.1056/NEJMra0912063.

Williams, A.L., S.B.R. Jacobs, H. Moreno-Macías, A. Huerta-Chagoya, C. Churchhouse, C. Márquez-Luna, H. García-Ortíz, M.J. Gómez-Vázquez, N.P. Burtt, C. a Aguilar-Salinas, C. González-Villalpando, J.C. Florez, L. Orozco, C. a Haiman, T. Tusié-Luna, and D. Altshuler. 2014. Sequence variants in SLC16A11 are a common risk factor for type 2 diabetes in Mexico. *Nature*. 506:97–101. doi:10.1038/nature12828.